Supramolecular Ordering of DNA in the Cholesteric Liquid Crystalline Phase: An Ultrastructural Study

Amílie Leforestier and Françoise Livolant
Centre de Biologie Cellulaire, 67 rue Maurice Günsbourg, 94205 Ivry-sur-Seine, Cedex, France

ABSTRACT Aqueous solutions of 146-base pair DNA fragments form a cholesteric liquid crystalline phase in the range of about 160–290 mg/ml. We present a structural analysis of this phase by comparing the data obtained from polarizing and electron microscopy. This phase shows multiple aspects or "textures" which are presented and interpreted. They mainly depend on the orientation of the structure relative to the observation plane and on the nature, distribution, and amount of defects present in the phase. These defects are then analyzed with the two methods, and the molecular orientations can be defined precisely in their core. The biological interest of such structural analyses is discussed in relation with the understanding of chromatin structure and function.

INTRODUCTION

The DNA molecule is densely packed in chromosomes, bacterial nucleoids, sperm heads, or virus capsids. Locally, the DNA concentration can vary from about 50 to 800 mg/ml according to Kellenberger et al. (1). In the same range of concentration, DNA forms in vitro liquid crystalline phases that are also highly ordered structures. Their nature depends on the polymer concentration (2–19). At low concentration, the DNA molecules are randomly oriented and the solution is a classical isotropic liquid. As the concentration gets higher, molecules order in the liquid that transforms into a liquid crystal of the "cholesteric" type (6, 7) and turns itself into a "columnar hexagonal" phase for higher concentrations (17, 18). Similar organizations can be found in vivo: a cholesteric organization of DNA was described in dinoflagellate chromosomes (6, 20, 21) and in certain bacterial nucleoids (22), and a hexagonal packing of DNA molecules was found in bacteriophages (23) and in certain sperm heads (24–26). In these biological examples, chromatin is devoid of classical histones and does not present a nucleosomic structure. These liquid crystalline phases of DNA can thus be considered as models of simple chromatin organization, and our goal was to analyze the structure of these mesophases and to compare them with chromatin. By this way, we hope to understand to what extent the liquid crystalline properties of DNA are involved in the process of condensation of chromatin in the living cell. Therefore, the structure of these phases was investigated first in polarizing microscopy by comparison with other biopolymers (7, 10, 12) and recently in electron microscopy by using freeze-fracture methods (18, 21). We present here new results about the cholesteric phase, and we show how it is possible to correlate data from optical and electron microscopy and how these two methods complement each other to provide information from the local to the long-range organization. This analysis was permitted by significant improvements of the methods: preparation of the DNA (well defined length of DNA fragments versus sonicated DNA) as well as methods of freezing and fracturing in electron microscopy (27).

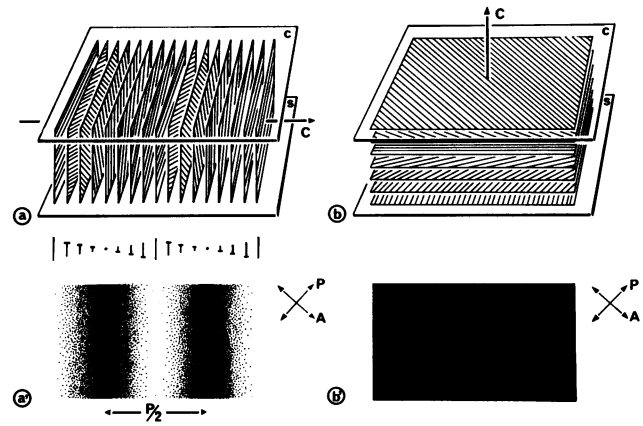

FIGURE 1 Different aspects of the cholesteric phase in polarizing microscopy. The cholesteric organization is schematically decomposed into a series of parallel and equidistant planes. In each of these planes the straight lines visualize the average DNA molecular orientation. This orientation rotates continuously from plane to plane along the cholesteric axis *C*. This supramolecular helical structure was shown to be left-handed. When a drop of the cholesteric phase is deposited between slide (*s*) and coverslip (*c*) different orientations of the cholesteric structure can occur. (*a*, *a'*) When the cholesteric axis (*C*) is lying in the preparation plane, molecules present different orientations relative to the preparation plane, alternatively parallel, oblique, and normal. In the top view, these orientations can be represented by lines (molecules parallel to the observation plane), nail-shaped marks (molecules oblique to the observation plane), and points (molecules normal to the observation plane). The tip of each nail indicates the extremity of the molecule that points toward the observer. Between crossed polars (*P*, *A*), the transmitted light is maximum for molecules lying in the preparation plane and minimum for molecules normal to this plane. A regular alternation of white and dark lines is observed, the periodicity corresponding to a rotation of 180° of the molecular orientations (i.e., *P*/2). (*b*, *b'*) When the cholesteric axis is normal to the preparation plane, molecules remain parallel to the planes of slide and coverslip and present all possible orientations. This apparent disorder leads to an extinction of the preparation between crossed polars.

Finally, the biological interest of understanding the structure of these mesophases will be discussed. Indeed, condensed states of DNA were considered for many years as

Received for publication 5 November 1992 and in final form 2 April 1993.

0006-3495/93/07/56/17 $2.00

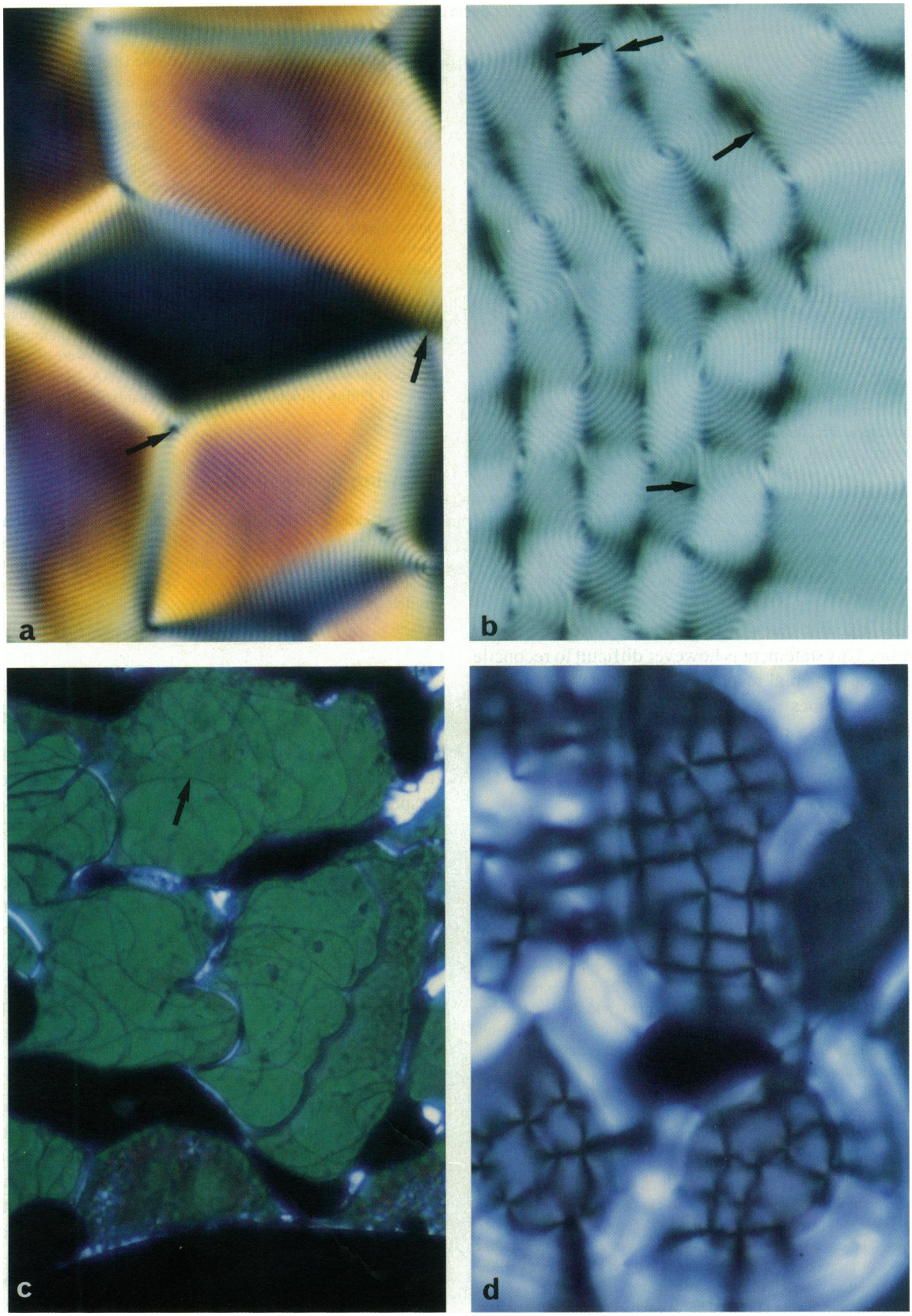

FIGURE 2 Multiple aspects of the DNA cholesteric phase in polarizing microscopy. DNA is dissolved in TE buffer (*a*), O.1 M NaCl (*b*), or 0.25 M ammonium acetate, 10 mM sodium cacodylate and 0.5 mM EDTA (pH 7) (*c* and *d*). (*a* and *b*) "Fingerprint patterns" with their alternation of bright and dark stripes. The stripes may present different orientations thus forming domains (*a*) or may be coiled to form spiralized patterns (*b*). These aspects are determined by the presence of defects (*arrows*). Regular undulations of the layers are also encountered sometimes (*b*, right part). (*a*, × 847; *b*, × 955, crossed circular polars). (*c*) "Planar textures" in domains limited by air (in *black*). The colors reveal the very small helical pitch of the cholesteric structure. The white areas correspond to unresolved fingerprint patterns interspersed in the planar texture. Numerous defect lines exist in the phase. They can be seen in the top view moving in the sample in planar textures (*arrow*) (× 955, crossed linear polars). (*d*) "Quadratic polygonal field texture" emerging from a planar texture (× 2360, crossed linear polars).

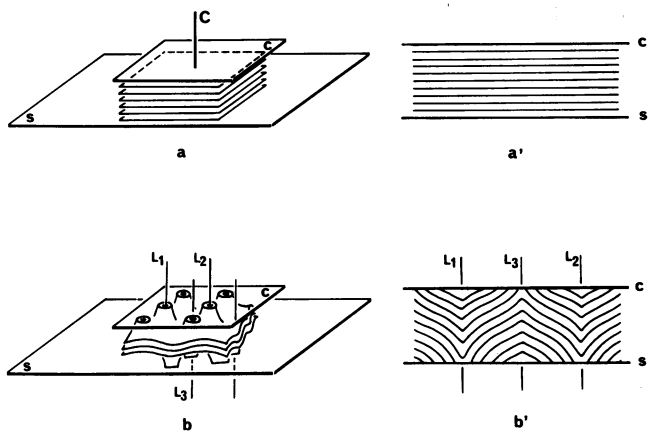

FIGURE 3 Transformation of planar textures (*a*) into polygonal textures (*b*). The cholesteric structure is schematized by a series of parallel planes separated by half the helical pitch *P*/2. In the planar texture (*a*), the layers lie parallel to the plane of the slide (*s*) and coverslip (*c*). The undulation of the layers occurs with formation of a periodic distribution of domes and basins. The layers now present a very strong curvature along focal lines (*L*) which are normal to the preparation plane (modified from Ref. 33). Sections normal to the preparation plane shows the parallel alignment of layers in planar textures (*a'*) and their regular distortion in polygonal textures (*b'*).

functionally inactive states of DNA, either in replication or transcription. This statement is however difficult to reconcile with recent experimental results showing that condensation of DNA in vitro does not prevent but on the contrary increases its activity in replication (28), recombination (29), and transcription (49).

MATERIALS AND METHODS

DNA preparation

Large amounts of DNA fragments about 500 Å in length (146 base pairs (bp)) were prepared by selective digestion of calf thymus chromatin with micrococcal nuclease according to the procedure described by Strzelecka and Rill (13). The length of the DNA fragments was checked by comparison with a 123-bp DNA ladder by polyacrylamide gel electrophoresis. Purified DNA was dissolved in various solvents, mainly in 0.25 M ammonium acetate, 10 mM sodium cacodylate, 0.5 mM EDTA (pH 7) and also in TE buffer (1 mM EDTA in 10 mM Tris-Cl^- buffer, pH 7.6) and in 0.1 M NaCl, at a concentration ranging from 150 to 250 mg/ml. Under these conditions, the liquid crystalline phase is cholesteric.

Polarizing microscopy

A 5–20-ml drop of the DNA solution was deposited between slide and coverslip leading to a sample thickness ranging from about 10–50 μm. Slides and coverslips were usually cleaned in ethanol/acetic acid solution (2:1, v/v) and carefully washed in distilled water. They were not treated in any other way. The coverslip was sealed to allow the solution to stabilize for a few hours or a few days. In some cases, a progressive increase in the polymer concentration was first obtained by a controlled evaporation of the solvent. The preparations were observed between linear crossed polars in a Nikon Optiphot X Pol microscope. Circular crossed polars were sometimes used to avoid the presence of black crosses that hinder the observation of the cholesteric layers.

Electron microscopy

For electron microscopy, DNA was dissolved in 0.25 M ammonium acetate, 10 mM sodium cacodylate, and 0.5 mM EDTA (pH 7). A comparative analysis of different cryofixation methods showed that best results were obtained by quick-freezing against a copper block cooled down to liquid helium temperature, in the absence of any cryoprotectant (27) in a Reichert-Jung cryovacuoblock device (after Ref. 30). Samples were settled onto copper discs and allowed to stabilize for 2–5 min at room temperature. The discs were stuck with double-sided adhesive paper on a Teflon cupel 1.1 mm in depth and projected onto the copper block (−291°C). The Teflon cupel acts as a check to avoid the complete squashing of the sample. These were immediately transferred and stored in liquid nitrogen. Freeze-fracture experiments were carried out in a Balzers BAF 400 T apparatus at −110°C under a 266.644-Pa vacuum. Samples were fractured with a razor blade in their upper 10 μm. After a 2-min etching at −100°C, the surface of the replica was unidirectionally shadowed with platinum/carbon at an angle of 45° and carbon-coated. The thickness of the deposit (20-Å platinum and 200-Å carbon) was monitored with a quartz crystal. Replicas were separated from the sample and washed in distilled water, where DNA dissolves, and observed in a 201 Philips (Eindhoven, Holland) transmission electron microscope at 80 kV.

Drawing conventions

The molecular orientations are represented by lines, nail-shaped marks, and points when they are, respectively, parallel, oblique, and normal to the observation plane. The tip of the nail corresponds to the extremity of the molecule that points toward the observer. Its length corresponds to the projection of a unit segment onto the observation plane.

RESULTS

Cholesteric textures in polarizing microscopy

DNA liquid crystals are viscous solutions in which molecules are ordered, while keeping their ability to slide the ones with respect to the others. The cholesteric phase is observed at room temperature in the range of 160 to about 290 mg/ml (19). It may coexist with the isotropic phase or with the more concentrated columnar hexagonal phase depending on DNA concentration and supporting electrolyte concentration. In the cholesteric phase, molecules are aligned in parallel, and their orientation rotates continuously along a direction which is called the cholesteric axis. This structure is helical and continuous, and for clarity a series of parallel and equidistant planes can be drawn (Fig. 1). This supramolecular helical structure was shown to be left-handed (31).

However, this phase presents multiple aspects (or textures) in polarizing microscopy, which are illustrated on Fig. 2. This polymorphism is due for one part to the orientation of the cholesteric axis relative to the preparation plane and, for the other part, to the nature, relative amount, and mutual arrangement of defects in the phase. Let us first consider the orientation of the cholesteric layers relative to the preparation plane.

Between crossed polars, the cholesteric phase frequently shows periodic alternations of light and dark stripes (Fig. 2, *a* and *b*). These patterns are observed when the cholesteric axis lies more or less parallel to the observation plane, as explained in Fig. 1 *a*. In these conditions of observation, the transmitted light is maximum when molecules are lying in the preparation plane and minimum when they are perpendicular to this plane. Other orientations produce intermediate levels of illumination. Therefore, the observed periodicity

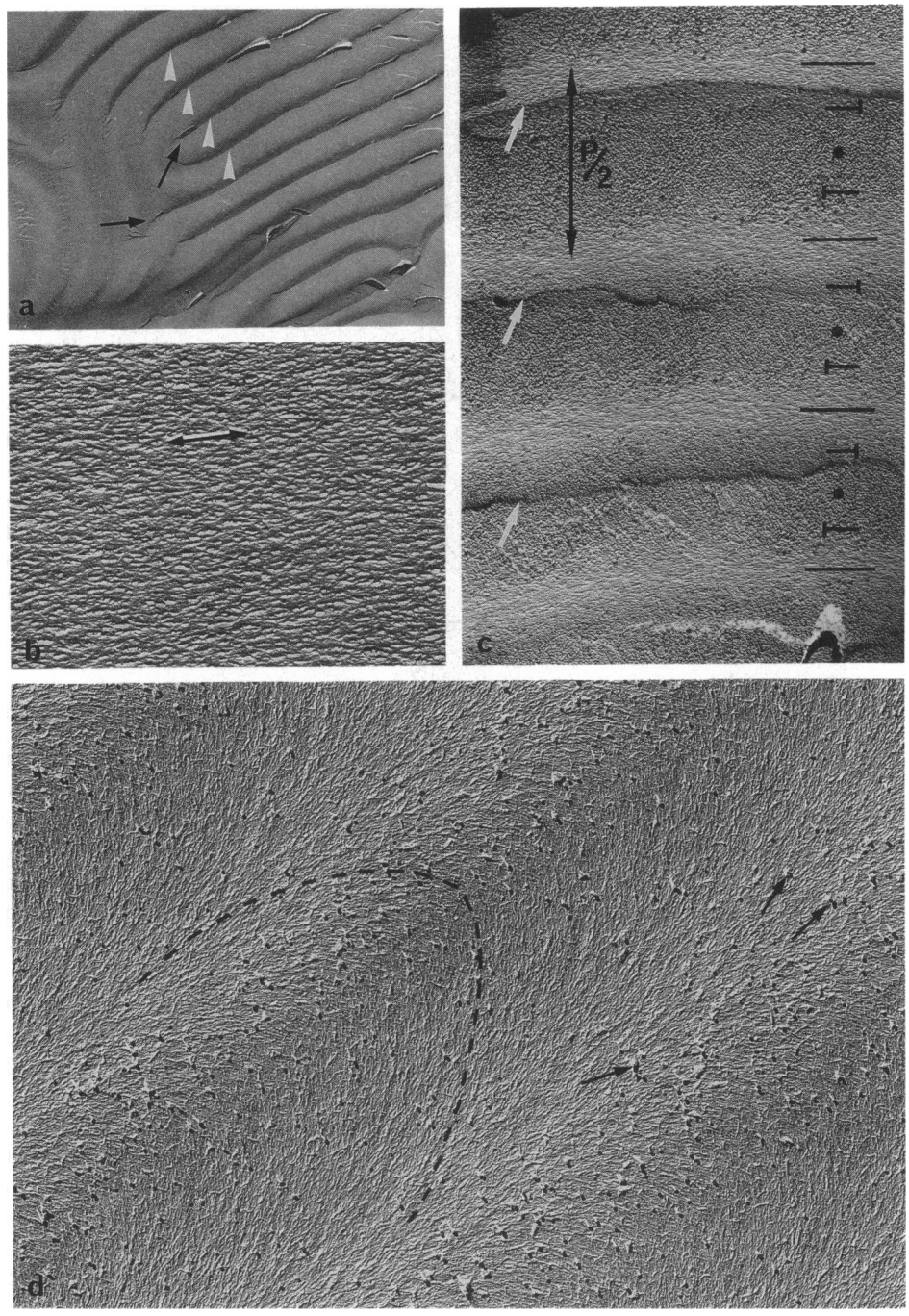

FIGURE 4 Different aspects of the cholesteric phase in electron microscopy. (*a*) General view of the cholesteric phase at small magnification, with periodic reliefs (*white arrows*). These patterns recall the fingerprints observed in polarizing microscopy. Structural defects can be recognized (*arrows*) (× 4,500). (*b–d*) Three different kinds of patterns can be recognized at higher magnification and correspond, respectively, to fracture planes normal (*b*, × 39,400), parallel (*c*, × 18,400), and oblique (*d*, × 18,400) to the cholesteric stratification. In (*b*) DNA molecules are unidirectionally aligned with a visible local disorder around the average orientation (*double arrow*). In *c*, periodic patterns are observed. They correspond to the regular alternation of molecules parallel, oblique, and normal to the fracture plane (*underlined*, respectively by *lines*, *nail-shaped marks*, and *points*). Half the helical pitch (*P*/2) can be measured on such micrographs. Fracture reliefs are underlined by white arrows. In *d*, a series of nested arches is drawn by the regular rotation of the molecular orientations. Some molecules were torn off during the fracture process, and they are strongly enhanced by the shadowing (*arrows*).

corresponds to half the helical pitch of the structure (*P*/2). The orientation of the cholesteric axis can change in the preparation plane, because of the presence of defects, leading to the well-known "fingerprint patterns." Some of these defects are indicated by arrows in Fig. 2, *a* and *b*.

Some regions of the preparation do not show these typical periodic patterns but instead more or less extinguished domains. In this case, the cholesteric axis lies normal to the preparation plane (Fig. 1 *b*). Molecules are then parallel to the observation plane and present all possible orientations because of the helical structure. Such textures are called "planar." They are usually more or less dark between crossed linear polars. In the same conditions of observation, these textures sometimes present very beautiful colors that cannot be extinguished by rotating the stage of the microscope (Fig. 2 *c*). They do not correspond to colors of birefringence but to a transmission of circularly polarized light in the visible spectrum. Thin lines can be seen moving in such planar preparations. They correspond to overhead views of defect lines (Fig. 2 *c*).

The occurrence of fingerprint or planar texture mainly depends on anchorage conditions of molecules on the glass slides. We did not control precisely the conditions required to get specifically one or the other texture. Nevertheless, we

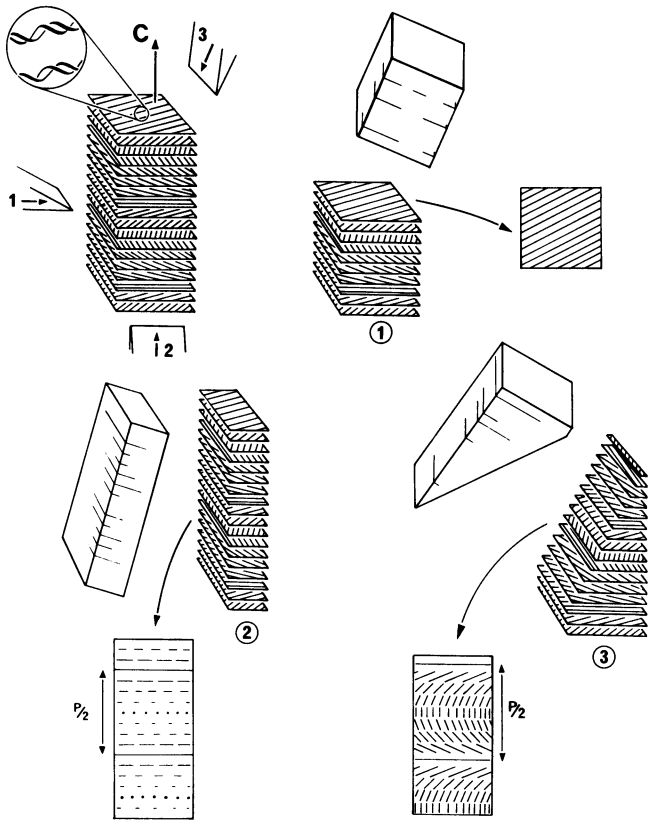

FIGURE 5 Origin of the different patterns on freeze-fracture replicas of the cholesteric phase. In a schematic drawing of the cholesteric organization, DNA molecules (represented by *lines*) are aligned in parallel in a series of fictive parallel equidistant planes. Their orientation rotates continuously along the cholesteric axis *C*. We considered three theoretical fracture planes, either normal (*1*), parallel (*2*), and oblique (*3*) to the cholesteric axis *C*. When the fracture plane is normal to the cholesteric axis (*1*), it follows more or less the molecular orientations, and a unidirectional orientation of molecules is expected. When the fracture plane is parallel to the cholesteric axis (*2*), all possible molecular orientations will be encountered in the fracture plane. The expected pattern is periodic with an alternation of molecules parallel, oblique, and normal to the surface of the replica. When the fracture plane is oblique with respect to the cholesteric stratification (*3*), the molecular orientations will draw a series of nested arches. Their width corresponds to a rotation of 180° of the molecular orientations (*P*/2). These situations are purely theoretical since they do not take into account the fact that the fracture surface is not a plane but an irregular surface.

observed that molecules show a tendency to align parallel to the glass slides. This effect was even more obvious in the thinnest preparations.

Besides, the presence of structural defects introduces a diversity of aspects as follows, depending on their amount, their nature, and the regularity of their distribution.

1) A perfect alignment of the cholesteric layers, without any defect, is observed only exceptionally and in small domains. Nevertheless, the alignment of the cholesteric layers can be achieved under electric or magnetic fields (11, 19, 32), but numerous defects remain trapped in the structure.

2) Textures with spiralized patterns can be seen (Fig. 2 *b*). There is a regular distribution of defects called "disclinations," the nature of which will be detailed further. The size of the spiralized domains may vary strongly from one domain to another.

3) Polygonal fields are also observed in the DNA cholesteric phase (Fig. 2 *d*). As mentioned previously (7), these textures are not very frequent, compared to other polymer mesophases. They were observed in only about 5% of the preparations. They arise from planar textures, in regions of very small helical pitch. Two square lattices can be seen, one at the level of the slide, the other at the level of the coverslip. Closing the diaphragm leads to the superimposition of the two networks. The polygon apices in one network correspond to the polygon centers in the other and conversely (see Fig. 13, *a–c*). In these polygonal fields of DNA, the cholesteric periodicity is never resolved in the optical microscope. The organization of the cholesteric layers in such textures has been previously analyzed (7, 33). They arise from a periodic curvature of the cholesteric layers that form domes and basins (Fig. 3). The loci of maximum curvature of the layers correspond to focal lines. These virtual lines are normal to the observation plane.

Cholesteric patterns in electron microscopy

Since the first ultrastructural analysis of DNA cholesteric liquid crystalline organization (21), experimental conditions were significantly improved. First, freezing methods, by projection of the sample onto a copper block cooled down to liquid helium temperature (4K), prevents the formation of ice cystals, thus allowing a better preservation of the molecular organization (27). Nevertheless, this method also presents disadvantages, namely deformations of the cholesteric structure produced by the squashing of the sample onto the copper block. Such distortions, which geometrical analysis has been worked out (34) are never observed when the sample is frozen by immersion into a cryogen (not illustrated). We took great care to make sure that the data presented here correspond to the initial cholesteric structure: similar results were obtained in samples frozen by the other method but the resolution of the molecules was not good enough to permit such an ultrastructural analysis. Besides, in previous experiments (21), a small layer of the sample was sandwiched between two gold planchets and the fracture was obtained by separating them. Fractures parallel to the molecular planes were then much favored since the cholesteric layers align preferentially parallel to the planchets. A different method to fracture the sample is now performed, using a knife that allows all possible orientations of the fracture plane relative to the cholesteric stratification. Favorable experimental conditions were then put together to permit the analysis of the molecular organization.

The observation of the replicas at low magnification usually reveals periodic patterns (Fig. 4 *a*) that recall the fingerprint patterns in polarizing microscopy.

Higher magnifications lead us to recognize layers with arched patterns (Fig. 4 *d*) and cholesteric layers devoid of

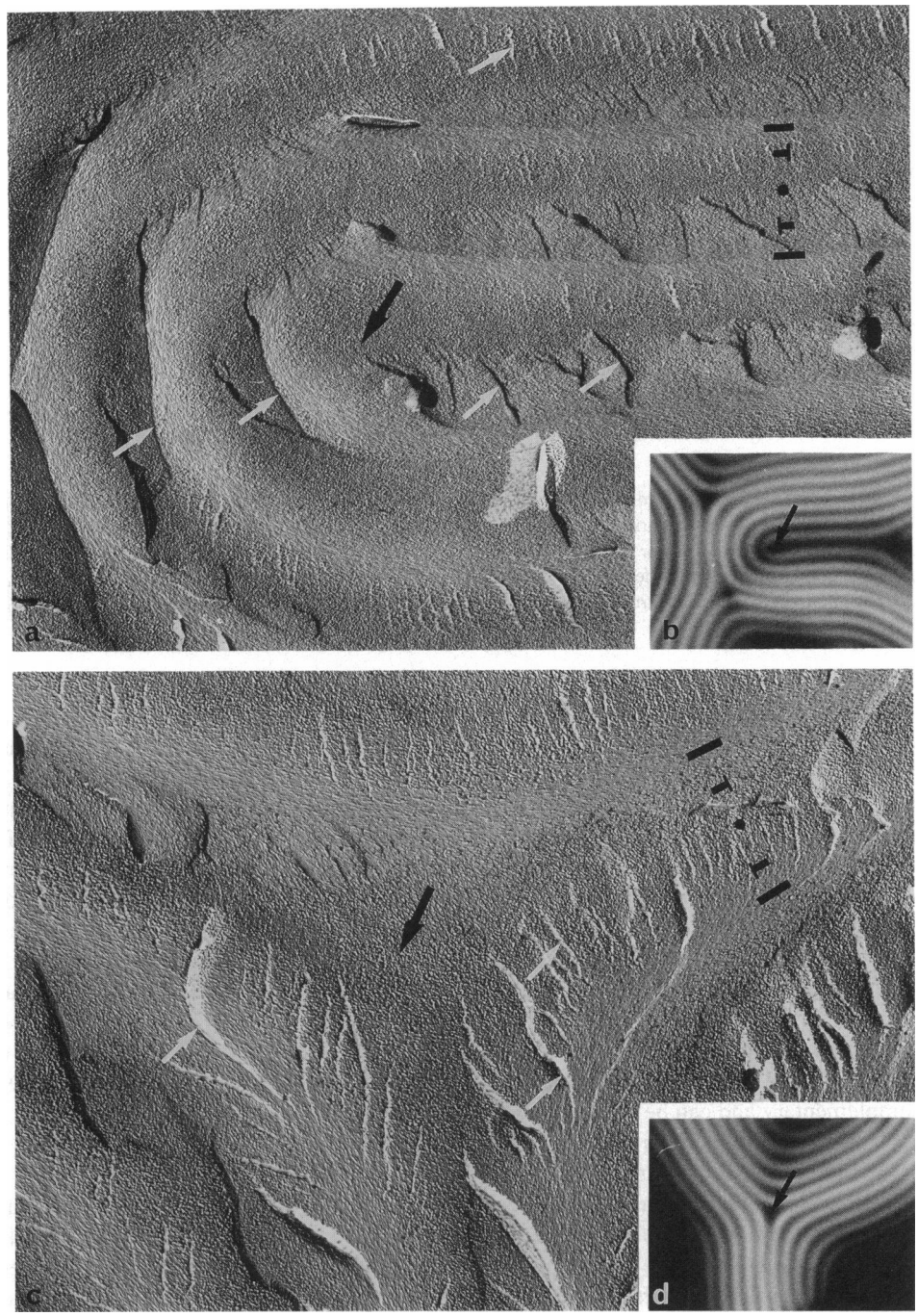

FIGURE 6 Defects in the cholesteric structure: $+\pi$ (*a* and *b*) and $-\pi$ disclinations (*c* and *d*). The molecular orientations are underlined by lines (molecules in the observation plane), nails (molecules oblique to the observation plane), and points (molecules normal to the observation plane). (*a*, *b*) Folding of the cholesteric layers corresponding to a rotation of 180° of the molecular orientations around a virtual line perpendicular to the observation plane (*black arrow*). The same defect is observed in electron microscopy (*a*) and in optical microscopy, between crossed circular polars (*b*). This defect corresponds to a $+\pi$ disclination with a λ core (see Fig. 7 *a*) (*a*, × 11,800; *b*, × 1,050). (*c*, *d*) Triple-point patterns observed in electron microscopy (*c*) and in polarizing microscopy (*d*). There is a rotation of 180° of the molecular orientations around the defect line (*black arrow*); it is a $-\pi$ disclination with a λ core (see Fig. 7 *c*) (*c*, × 18,750; *d*, × 1,050). In both cases, molecules lie parallel to the defect line in the core of the defect. White arrows on the freeze-fracture micrographs indicate the steps due to the fracturing process.

arches (Fig. 4 *c*). It is possible to follow precisely the molecular orientations within each layer (parallel, oblique, or normal to the fracture plane). These orientations have been underlined, respectively, by lines, nail-shaped marks, and points to help the reader (Fig. 4 *c*). These are also regions devoid of any periodicity (Fig. 4 *b*) in which a unidirectional alignment of molecules can be recognized. These patterns arise from the orientation of the observation plane (here the fracture plane) relative to the cholesteric axis. There are three main possible orientations, either parallel, oblique, and normal to the cholesteric axis, as explained in Fig. 5. The fracture plane parallel to the cholesteric axis shows periodic patterns with an alternation of DNA filaments parallel, oblique, and normal to the fracture plane. Oblique fracture planes are manifested as a series of nested arches appearing inside each layer; these arches are created by the successive orientations of DNA molecules along the cholesteric axis. Each layer (with or without series of arches) corresponds to a rotation of 180° of the molecular orientations (i.e., to *P*/2). When the fracture plane is more or less normal to the cholesteric axis, it follows the molecular alignment and there is no visible periodicity.

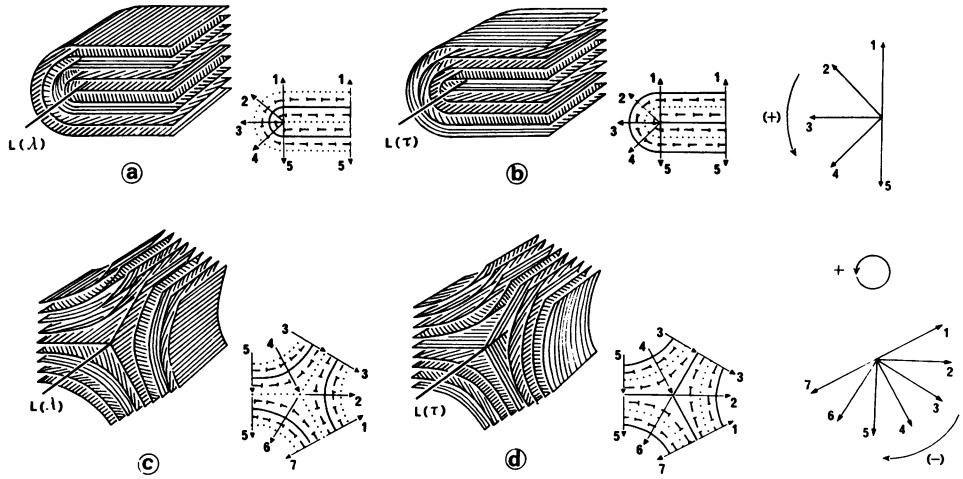

FIGURE 7 Different types of disclinations drawn in perspective with their schematic representation. (*a*, *b*) Folding of the layers around the defect line (*L*) with the molecules either parallel to this line in the core of the defect (λ line) (*a*) or normal to this line (τ line) (*b*). In both cases, a vector normal to the cholesteric layers rotate by π (from position *1* to *5*) in the trigonometric direction (which is positive by convention). These are $+\pi$ disclinations. (*c*, *d*) Triple-point patterns around defect lines (*L*). Molecules are either parallel (λ line) (*c*) or normal (τ line) (*d*) to the defect line in the core of the defect. Along a circuit in the trigonometric direction, the vector normal to the cholesteric layers rotates by π in the opposite direction (from position *1* to *7*). These are $-\pi$ disclinations.

The observation plane defined by the fracture is in fact a very irregular surface, that presents two kinds of reliefs. The first ones, of small amplitude, are due to the molecules themselves, as already mentioned. The second ones are more important; they are underlined by white arrows on the micrographs. They correspond to steps of variable height, the formation of which depends on the direction of the knife pass relative to the orientation of the cholesteric structure. These steps can be either parallel, oblique, or normal to the cholesteric stratification, and they underline the cholesteric periodicity. These reliefs may sometimes impede the observation of the molecular orientations.

Data obtained from these two microscopical methods are complementary and can be compared. In polarizing microscopy, the observed patterns come from the optical properties of the sample, depending on the orientation of the molecules in the thickness of the preparation, whereas in freeze-fracture electron microscopy, we observe the surface of a fracture within the sample and we can follow the molecules themselves at the surface of the replica. In both cases, the periodic patterns correspond to half the helical pitch *P*/2. In addition, the patterns depend on the orientation of the cholesteric axis relative to the observation plane (preparation plane in polarizing microscopy and fracture plane in electron microscopy). The structural analysis of this phase can then be driven fruitfully in parallel with the two methods, namely the analysis of the defects that exist in the structure.

Defects of the cholesteric phase

Liquid crystalline phases present numerous defects that can be either points, lines, or walls (35). Some defect lines are easily followed in planar textures, when the cholesteric layers are lying parallel to the planes of slide and coverslip (Fig. 2 *c*). These defects can be seen in "cross-section" when the cholesteric structure is rotated by 90°, with the cholesteric axis lying in the preparation plane. They can appear either as bifurcating lines (either dark or bright) called "dislocations" or points around which the molecular orientations rotate, called "disclinations." The optical analysis of these defects was previously considered with sonicated DNA, in comparison with the defects observed in other biopolymers mesophases (7). We present here an analysis of these defects in polarizing microscopy and also in electron microscopy which permits a direct access to the molecular organization along their core. Moreover, this analysis was performed with short DNA fragments, and differences can be noticed between short and long DNA fragments.

Disclinations

Disclinations can be found in regions of strong curvature of the cholesteric layers. In fingerprint patterns, they can be seen in "cross section" either as the locus around which cholesteric layers are folded (Fig. 6 *b*) or as the core of triple-point patterns (Fig. 6 *d*). In both cases, the cholesteric layers rotate by 180° around these lines, but this rotation is considered, by convention, to be either positive or negative, as explained in Fig. 7. Therefore, these defect lines are called, respectively, $+\pi$ or $-\pi$ disclinations.

In both cases, two theoretical situations are possible since the molecular orientations can be either parallel or perpendicular to this line in the core of the defect. When molecules lie parallel to the defect line, there is no discontinuity in the molecular orientations; the line is called λ. The alternate situation, with molecules normal to the defect line in the core, corresponds to τ lines. In polarizing microscopy, the cores of the defects are dark, meaning that the molecules lie parallel to the microscope axis, thus parallel to the defect line. The defects are, respectively, λ^+ (Fig. 6 *b*) and λ^- (Fig. 6 *d*). The

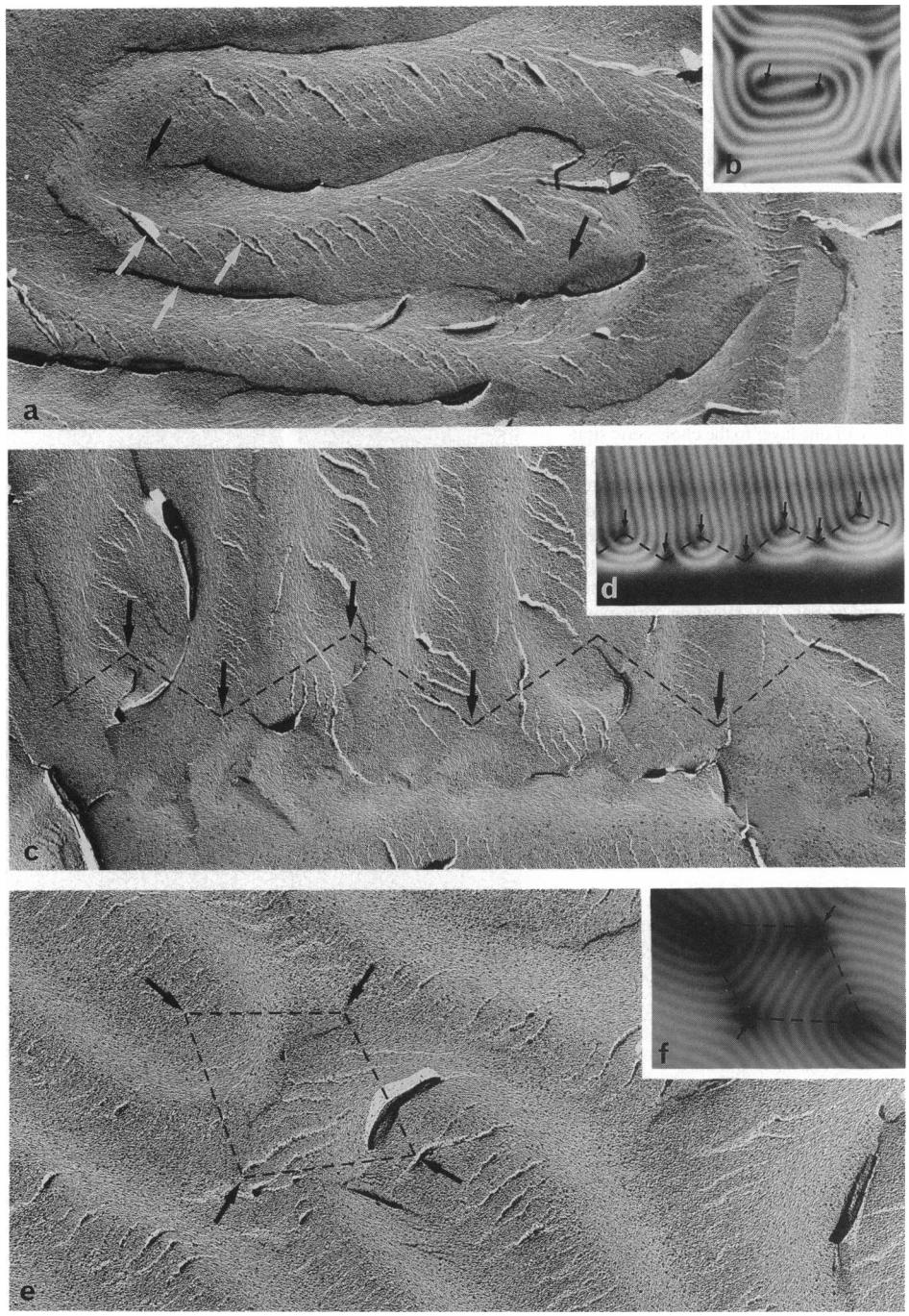

FIGURE 8 Defects in the cholesteric structure: association of numerous disclinations observed in electron microscopy (*a*, *c*, *e*) and in polarizing microscopy (*b*, *d*, *f*). (*a*, *b*) Flattened double spiral patterns formed by the association of two $+\pi$ disclinations, the cores of which are indicated by the black arrows (*a*, × 8,400; *b*, × 1,050). (*c*, *d*) Alternation of $+\pi$ and $-\pi$ disclinations. The line joining the opposite sign disclinations (indicated by the black arrows) draws a zig-zag line (*c*, × 8,400; *d*, × 1,230). (*e*, *f*) Combination of two $+\pi$ and two $-\pi$ disclinations (the cores of which are indicated by the *black arrows*) draws a quadrilateral pattern (*e*, × 13,100; *f*, × 1,300). White arrows underline reliefs which are produced by the fracture process.

same defects are observed in electron microscopy, and the molecules themselves can be seen normal to the section plane, i.e., parallel to the defect line in the core of the defect (Fig. 6, *a* and *c*). In these examples, the situation is quite simple, since the fracture plane is perfectly normal to the cholesteric stratification. This situation is rare. In the general case, the fracture plane is more or less oblique to the cholesteric stratification, and to the defect line. Then, the basic pattern remains the same (triple point or folding of the layers), but the obliquity is manifested as a series of nested arches appearing in the cholesteric layers. Moreover, in the vicinity of the core, molecular orientations seem to follow different arrangements, but these patterns depend in fact on the orientation of the fracture plane (36). These aspects will be illustrated further in the case of dislocations.

These disclinations can combine to form different patterns, as illustrated in Fig. 8. Pairs of associated $+\pi$ disclinations form flattened double spirals (Fig. 8, *a* and *b*) that can be recognized in polarizing and electron microscopy. The regular alternation of $+\pi$ and $-\pi$ disclinations leads to the appearance of two domains of different orientations of the cholesteric layers, separated by a zig-zag line joining the cores of opposite sign disclinations (Fig. 8, *c* and *d*). This zig-zag line can be effectively seen between linear crossed

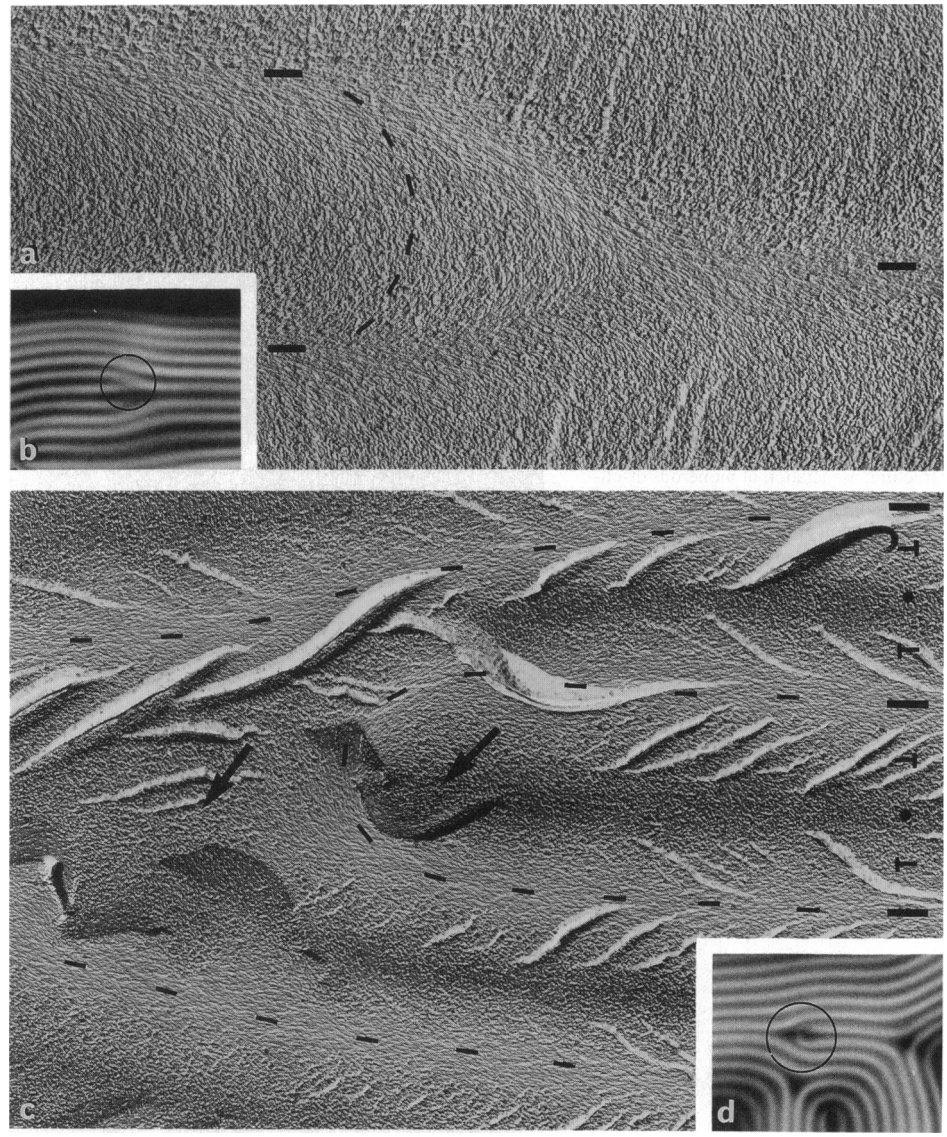

FIGURE 9 Defects in the cholesteric structure: edge dislocations observed in electron microscopy (*a* and *c*) and in polarizing microscopy (*b* and *d*). (*a*, *b*) Addition of one layer to the cholesteric stratification (**b** = *P*/2). In *b*, a white line divides into two which corresponds to a $\tau^-\lambda^+$ core. The same defect is observed in *a* with the fracture plane slightly oblique with respect to the cholesteric stratification, which is manifested in a series of nested arches. This situation corresponds to Fig. 11 *a1* (*a*, × 18,750; *b*, × 1,050). (*c*, *d*) Addition of two layers to the cholesteric stratification (**b** = *P*). The defect is $\lambda^-\lambda^+$ (with molecules parallel to the two associated defect lines (*black arrows*) (*c*, × 18,750; *d*, × 1,050).

polars (37). Square patterns are also formed by the association of two $-\pi$ and two $+\pi$ disclinations (Fig. 8, *e* and *f*).

Dislocations

Dislocations are translation defects and correspond to the addition (or removal) of one or a few layers in the cholesteric structure. Two examples of such defects are presented in Fig. 9 in polarizing and in electron microscopy. These dislocations are defined by a vector **b** (the Burgers' vector) that corresponds to the number of added layers. Each layer corresponds to *P*/2, i.e., to a rotation of 180° of the director.

Edge dislocations can be considered as the association of two disclination lines of opposite sign. These lines, that run parallel to each other, and normal to the cholesteric stratification, are distant of $nP/4$, with $n = 1, 2$, and 3 for one, two, or three layers added. Considering that the molecules can theoretically be either parallel (λ) or perpendicular (τ) to the axis of the defect line in the core of each disclination, two situations are possible in the core of the edge dislocation for each value of the Burgers' vector. For odd numbers of added layers, the two disclination lines are of different type (one τ and one λ), whereas they are of the same type (two τ or two λ) for even numbers of layers (Fig. 10).

As mentioned previously, a given defect can present different aspects according to the orientation of the fracture plane relative to the cholesteric stratification and defect line. Different situations are analyzed in Fig. 11 in the two cases corresponding to the addition of one layer (**b** = *P*/2). The stratification is devoid of arches when the fracture plane is perpendicular to the stratification. Any other orientation of the fracture plane results in the appearance of the typical arched patterns. However, their concavity can be oriented either toward the core of the defect (*planes 2* and *3* in Fig. 11) or in the opposite direction (*planes 1*), depending on the orientation of the fracture plane. Moreover, complex patterns, leading to symmetry breaking, appear when the fracture planes are oblique with respect to the cholesteric structure and to the defect line at once (*planes 3*). This analysis allows the interpretation of complex situations which can be

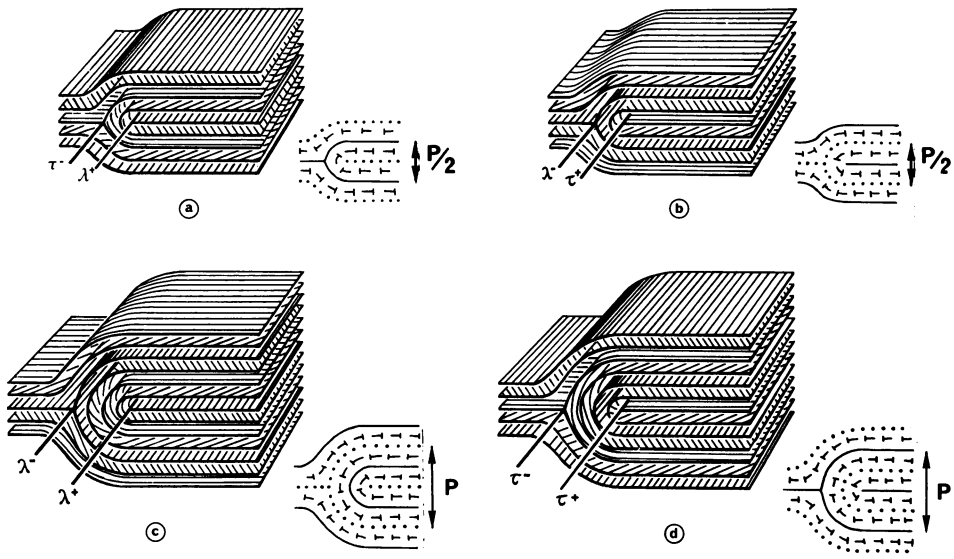

FIGURE 10 Different types of edge dislocations corresponding to the addition of one layer (**b** = *P*/2) (*a* and *b*) or two layers (**b** = *P*) (*c* and *d*) in the cholesteric structure. Each defect is presented in a perspective view and in the corresponding schematic representation.

encountered on fracture replicas and correspond in fact to classical molecular configurations in the three-dimensional space. For example, the pattern presented on Fig. 9 *a* is typical of a $\tau^-\lambda^+$ edge dislocation when the fracture plane is oblique to the cholesteric layers (case a_1 in Fig. 11). In polarizing microscopy, the same defect shows a white Y-shaped pattern (Fig. 9 *b*). The addition of two layers in the structure (**b** = *P*) is illustrated in polarizing microscopy (Fig. 9 *d*) and in electron microscopy, with the fracture plane normal to the defect line and to the stratification (Fig. 9 *c*). In this case, the defect is $\lambda^-\lambda^+$. However, this analysis was performed manually, point by point, and only a few possible patterns have been drawn. An exhaustive study would require data processing means.

Tables 1 and 2 show the occurrence of the different types of defects observed in the cholesteric phase. Although they are less numerous, the data collected in electron microscopy confirm those obtained in polarizing microscopy.

The disclinations are either $+\pi$ or $-\pi$ and the repartition between the two types seems to be equal even if the counting are not very large. $-\pi$ disclinations are exclusively of the λ type, whereas some $+\pi$ disclinations of τ type have been observed. The λ defects do not correspond to discontinuities in the molecular orientations and are therefore much more likely.

A total of 183 dislocations were analyzed in this phase. Defects corresponding to the addition of one or two layers are in equal amount, and together they represent more than 88% of the total dislocations. However, certain situations are more frequent than others. It appears that the association of frequent disclinations gives frequent dislocations: $\lambda^-\lambda^+$ are much more favored than $\tau^-\tau^+$ in the case **b** = *P*. When there is addition of one layer (**b** = *P*/2) there is always one τ line in the defect. As seen previously, the τ^+ disclination is not completely prohibited, and we observe that $\tau^+\lambda^-$ lines are more frequent than the $\tau^-\lambda^+$ lines.

The occurrence of defects observed on the one hand with monodisperse "short" DNA fragments (500 Å), and, on the other hand, with longer and sonicated DNA fragments (0.05–1.9 μm) (7) are presented in Fig. 12. Defects are of the same kind and their relative amount is quite the same except for *P*/2 dislocations: they are more numerous with long DNA fragments and $\tau^-\lambda^+$ lines are then more frequent than $\lambda^-\tau^+$ lines.

Curvature and distortions of the layers

In some preparations, the curvature of the layers is very regular, leading to special textures: textures with numerous double spirals (Fig. 2 *b*) and textures with regular undulations of the cholesteric layers (Fig. 2 *b*, right part). These textures are not encountered very frequently.

The "polygonal textures" (Figs. 2 *d* and 13 *a–c*) are also regions of strong curvature of the layers. As already mentioned, the cholesteric layers are periodically undulated in two orthogonal directions, leading to these typical patterns in polarizing microscopy. In this case, the lines of maximum curvature (focal lines) are normal to the observation plane (Fig. 3, *b* and *b'*). Fracture planes normal to these lines reveal patterns such as that illustrated in Fig. 13 *d*. Series of nested arches (characteristic of the cholesteric organization) are recognized. They draw a double spiral, that is not very easy to follow, because of the presence of fracture reliefs already mentioned (white arrows). These reliefs draw a single spiral which superimposes to the double spiral of arches. The origin of these patterns can be understood quite easily as explained in Fig. 14. The cholesteric layers are distorted into a dome and the fracture plane is normal to the axis of the deformation. The fracture reveals different levels of the cholesteric organization on which are drawn the molecular orientations (Fig. 14 *b*). In projection onto the observation plane, these different orientations of the DNA molecules draw a double spiral of arcs, the limits of which are underlined (Fig. 14 *c*). Such patterns are very frequently encountered with another biopolymer, xanthan, that forms a cholesteric mesophase in

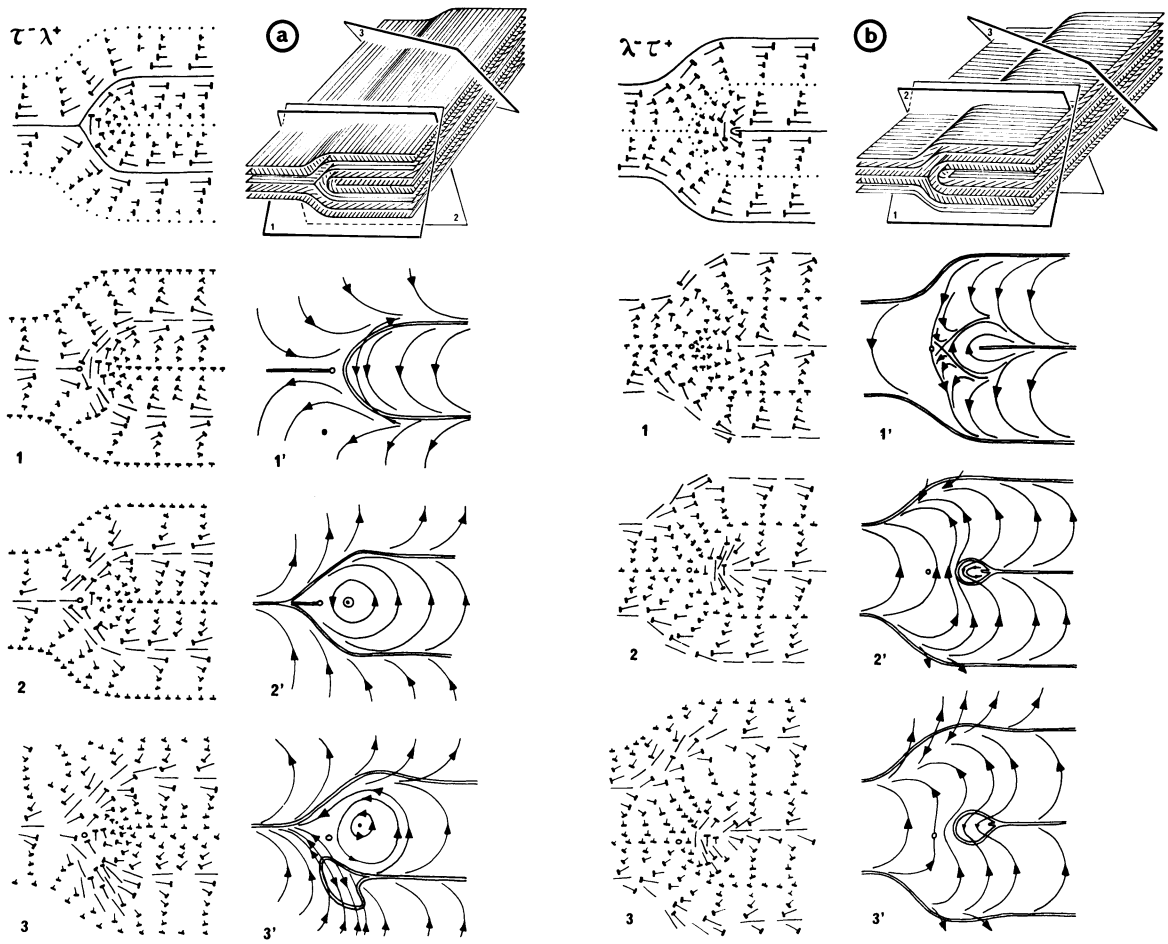

FIGURE 11 Geometrical analysis of the patterns observed for various orientations of the fracture plane relative to the edge dislocations $\tau^-\lambda^+$ (*a*) and $\lambda^-\tau^+$ (*b*). For each situation, two representations are given, either the nail convention that indicates the molecular orientation in each point and the arrowheads convention that allows an easier comparison with the observed patterns. (Note that in this latter case, double lines correspond to molecules lying in the section plane.) The core of the defect, which can be considered as a reference point is indicated by a small circle on each drawing. Though series of arches are always observed when the fracture plane is oblique to the cholesteric stratification, this analysis illustrates the diversity of patterns corresponding to a similar molecular configuration, due to different projections onto the observation plane.

aqueous solution and presents a high frequency of polygonal textures (7, 38).

Helical pitch

In fingerprint textures, the helical pitch P, measured directly on the micrographs, varies from about 1.5 to 3.5 μm with an average value of 2.54 μm $\pm$ 0.9 μm (s = 0.45). These measurements were done on 96 micrographs, in domains devoid of defects. The pitch does not seem to be dependent on the ionic species present in the buffer (P = 2.6 μm in TE buffer, 2.57 μm in ammonium acetate and 2.52 μm in NaCl). The pitch is about the same (P = 2.49 μm $\pm$ 0.9) in the cholesteric germs in equilibrium with the isotropic phase. These results were confirmed by measurements on electron micrographs in regions showing periodic patterns devoid of arches. It varies from 0.8 to 4 μm with an average value of 2.5 μm. These results are slightly different from the mean value of 2.2 μm $\pm$ 0.2 given by Rill and collaborators (19, 39). Moreover, we notice a larger distribution of data around the average value with a standard deviation s = 0.45. Taking into account that we did not use the same method, we cannot rule out the hypothesis that our results could be slightly biased since the pitch was measured on micrographs, which may introduce a subjective choice of the regions of interest. Nevertheless, we rule out the hypothesis of a selection of cholesteric areas near

TABLE 1 Disclinations

	−Π		+Π	
	λ^-	τ^-	λ^+	τ^+
146-bp DNA				
E.M.	16	0	11	1
P.M.	21	0	17	1
Total	37	0	28	2
Sonicated DNA (after Livolant (7))	+++	0	+++	ε

Counting of the disclinations observed in the cholesteric phase of DNA made of 146-bp fragments in polarizing microscopy (P.M.) and in electron microscopy (E.M.).

TABLE 2 Dislocations

	$p/2$		p		$3p/2$		$2p$	
	$\tau^-\lambda^+$	$\lambda^-\tau^+$	$\tau^-\tau^+$	$\lambda^-\lambda^+$	$\tau^-\lambda^+$	$\lambda^-\tau^+$	$\tau^-\tau^+$	$\lambda^-\lambda^+$
146-bp DNA								
E.M.	8	16	0	33	1	5	0	3
P.M.	15	42	3	45	1	3	0	8
Total	23	58	3	78	2	8	0	11
Sonicated DNA (after Livolant (7))	72	44	4	73	1	1	0	8

Counting of the dislocations observed in the cholesteric phase made of 146-bp DNA fragments in electron microscopy (E.M.) and in polarizing microscopy (P.M.). For each value of the Burgers' vector (**b** = $P/2$, P, $3P/2$, $2P$), the two possible situations in the core of the defect were differentiated.

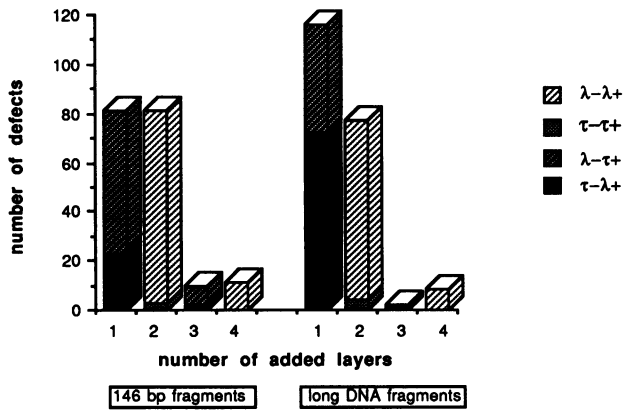

FIGURE 12 Histogram comparing the frequency of defects observed in the cholesteric phase of DNA when composed of short (146 bp) and long DNA fragments. For each number of added layers (*1* = $P/2$; *2* = P; *3* = $3P/2$; *4* = $2P$) the two situations in the core are considered (from data presented in Table 1).

the transition with the hexagonal phase since we obtain the same values in the cholesteric germs. Anyway, we agree with Rill and collaborators to say that there is no visible effect of the ionic species or concentration on the pitch.

We noticed local variations around this bulk value of the pitch that seem to be related to different effects: curvature of the layers, textures, and phase transitions.

Local variations related to the curvature of the layers

These variations of the pitch are easily visualized in the vicinity of defects. Their core is usually large (*black core* in Fig. 6 *d*, for example). The pitch can be measured along the line of maximum curvature of the layers and compared to the neighboring region of planar layers, which reveals a 40% increase of the pitch.

The curvature of the layers is sometimes too strong to afford a regular increase of the cholesteric pitch. Groups of cholesteric layers then separate and are interspersed by areas which appear black in polarizing microscopy. In such cases, the twist shows strong variations and is nearly prevented in some places along the line of maximum curvature (not illustrated).

We noticed similar variations of the cholesteric pitch in quadratic polygonal fields in which the checkerboard pattern is made of an alternation of pink and green squares. Such color differences reveal periodic variations of the helical pitch between domains of strong curvature of the layers. These domains are separated by focal lines. In half of these domains, the curvature of the layers tends to increase the twist between DNA molecules, whereas in other ones the curvature favors the untwisting of the structure.

Variations in relation with the textures

In planar and polygonal textures, the helical pitch is usually much smaller, and it is not resolved in polarizing microscopy. In some preparations (Fig. 2 *c*), the colors exhibited by domains with planar textures reveals that P can be as small as 0.2–0.4 μm. Indeed, the incident light, which can be considered as composed of two components of opposite circular polarizations, is parallel to the helical axis of the cholesteric structure and a Bragg reflection occurs. One component is strongly reflected, whereas the other one is transmitted. These two lights are circularly polarized but of opposite handedness. Their wavelength is proportional to the helical pitch of the structure according to the relation $\lambda_o = Pn$ (λ_o being the wavelength of the reflected light, P the helical pitch of the structure, and n the average refractive index of the sample). If n is about 1.5, the colors indicate that the pitch is ranging from 0.2 to 0.4 μm in these domains. The preparations showing these small cholesteric pitches are rather rare, which explains why they were never encountered on freeze-fracture replicas. Their occurrence requires particular conditions that we do not control. They undoubtedly correspond to high DNA concentrations, since they are always observed close to the transition with the more concentrated phase. They were observed with 146-bp DNA fragments (in the presence of NH_4^+ as a counterion) and with sonicated DNA (200–6000 bp) in the presence of K^+ ions (Plate IIIb in Ref. 7). However, we cannot determine the exact polymer and electrolyte concentrations: our experiments were not always performed with well-defined concentration samples but usually in preparations allowed to dry slowly to study the evolution of the liquid crystalline phases with polymer concentration. Van Winkle et al. (39) did not notice their occurrence over a wide range of DNA concentration and electrolyte concentration (from 130 to 300 mg/ml DNA and a supporting electrolyte concentration of 0.01–1.0 M NaCl and of 0.25 M ammonium acetate). They observed instead that

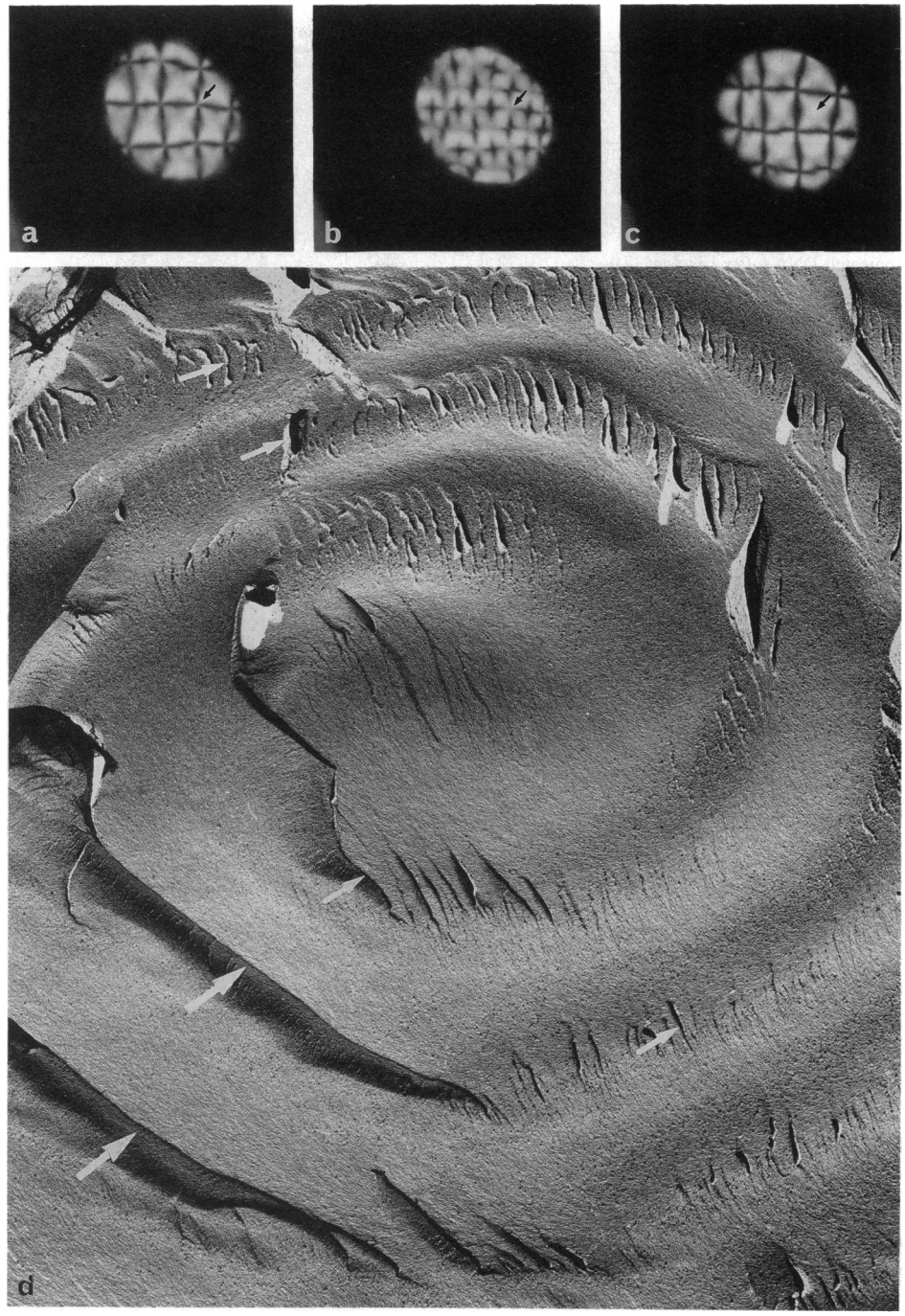

FIGURE 13 Distortions of the cholesteric layers observed in polarizing (*a–c*) and in electron microscopy (*d*). (*a–c*) Polygonal patterns observed in polarizing microscopy, between crossed linear polars. The same cholesteric domain, limited by air, is focused in the slide plane (*a*), in the coverslip plane (*c*), and in between (*b*). The arrow points to the same locus in the three cases (× 2,175). (*d*) Spiral pattern corresponding to a region of strong curvature of the cholesteric layers. The cholesteric layers form a double spiral (difficult to follow) that superimposes to a single spiral of relief (× 11,800).

the pitch was relatively independent of DNA concentration and electrolyte concentration. We suspect that these small pitch cholesteric phases are favored by a parallel alignment of DNA molecules to the glass slides, leading to the formation of planar textures, in very thin preparations. A systematic study of experimental conditions required to get these small pitch cholesteric phases remains to be done.

Variations related to the phase transition

We also noticed variations of the helical pitch that are related to the transition with the more concentrated hexagonal phase. Different mechanisms can be discerned. Usually, the transition occurs by nucleation and growing of hexagonal germs in an undistorted cholesteric phase (40). Then, the pitch increases only slightly to reach a mean value of 3.67 μm as measured in electron microscopy. Other transition processes are also observed. Around 15% of the samples display a strong untwisting of the cholesteric phase, with the helical pitch reaching values as high as 5–10 μm, as mentioned previously by Van Winkle et al (39). Lastly, the transition can also occur in the rare regions of very small helical pitch (0.2–0.4 μm). The detailed analysis of this phase transition is in progress.

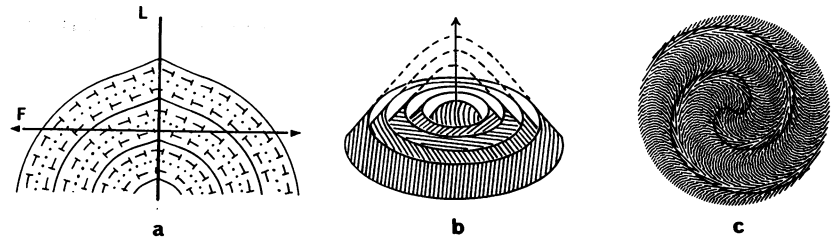

FIGURE 14 Origin of double spiral patterns. The cholesteric layers are distorted to form a dome (*a*), and the fracture plane *F* is normal to the line of maximum curvature of the layers *L*. After fracturing, the different molecular orientations are observed in the superimposed layers of the cholesteric structure (*b*). In projection onto the observation plane, the molecular orientations draw a double spiral of arches (*c*).

DISCUSSION

For a long time, condensed chromatin has been considered as inactive and therefore of poor interest from a biological point of view, but numerous data are now available which indicates that DNA replication and genetic recombination, instead of being inhibited, are stimulated by DNA condensation (28, 29, 41). More precisely, the rate of DNA synthesis by DNA polymerase is increased, probably by stabilization of the DNA-polymerase complex (42). The activity of type I and type II topoisomerases is significantly increased (43), as well as the intermolecular DNA ligation reactions (44). In addition, DNA condensation is able to favor strand exchange reactions without the addition of any protein (29). Besides, renaturation reaction efficiency is increased, from 25% in the isotropic phase to 80% in the cholesteric liquid crystalline phase (45).

To understand how DNA functions in this condensed state, it appears crucial to know what its supramolecular organization is, and liquid crystalline phases represent good models (however simple they may be) to study the order that spontaneously occurs between DNA molecules. Indeed, these phases ally three properties which are probably required for DNA to function: high local DNA concentration (to facilitate the contacts between molecules), fluidity of the structure (to help the components of the reaction to come into contact), and order between molecules (which is required in certain reactions, like homologous pairing). The aim of this study was to consider the DNA ordering at short- and long-range distance but also the deviations from this order, i.e., the defects, which are themselves highly elaborated and ordered structures.

TABLE 3 Comparison of the defects observed in vitro and in chromosomes

	disclinations	edge dislocations			
	$-\pi$	b = P/2		b = P	
		$\lambda^-\tau^+$	$\tau^-\lambda^+$	$\tau^-\tau^+$	$\lambda^-\lambda^+$
DNA *in vitro* (500 Å)	λ^-	58	23	3	78
DNA *in vitro* (500 Å to 3 μm)	λ^-	44	72	4	73
chromosomes	τ^-	13	44	-	2

The shading indicates situations which are compatible only with an antiparallel alignment of the DNA molecules.

Defects and their significance

Defects are well known to be involved in crystal growth, and some of those studied here happen to be preferential sites of nucleation of the more concentrated liquid crystalline phase (40). The precise analysis of their role in the phase transition process is in progress. Besides, from a biological point of view, we may hypothesize that these defects are also of some

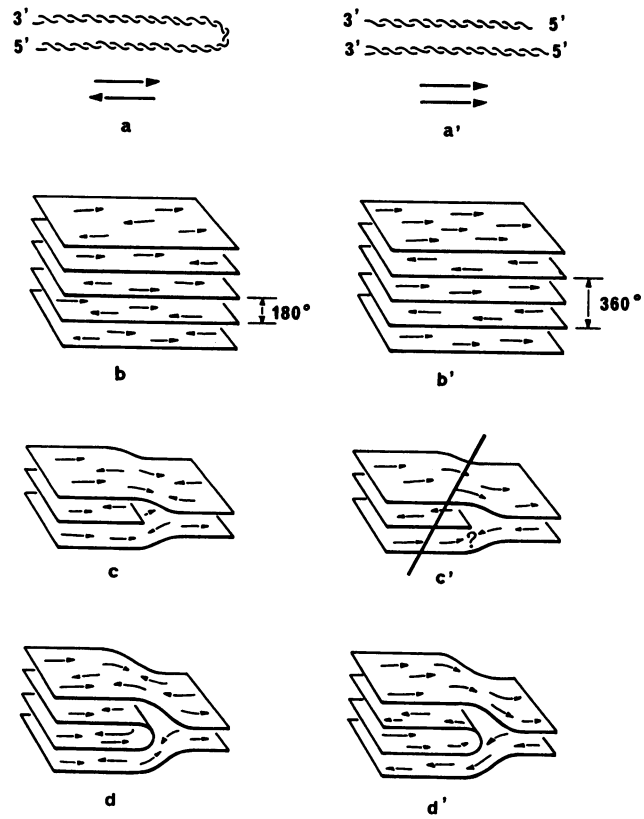

FIGURE 15 Relationship between the constraints of alignment of the DNA molecule and the nature of the defects in the cholesteric phase. Two situations are considered: the DNA molecule can fold and go back and forth, the polarity of the DNA molecule (taken arbitrarily on one strand) is not taken into account (*a*) or DNA molecules must align strictly in parallel (*a'*). In the cholesteric structure, represented by a series of planes separated by a rotation of 180° of the molecular orientations, the true period corresponds then to *P*/2 (180° rotation) in the first case (*b*) and to *P* (360° rotation) in the other one (*b'*). Consequently, a defect with a Burger's value, **b** = *P*/2, is possible in the first hypothesis (*c*), whereas it is prevented in the alternative (*c'*) since it would introduce an antiparallel alignment of molecules. Defects with a Burger's vector, **b** = *P*, are allowed in both hypotheses (*d*, *d'*).

importance in the activity of chromatin in vivo. Some elements do support this hypothesis.

1) First, the defects described in this article are also observed in living cells, namely in dinoflagellate chromosomes in which they were analyzed in detail (6). Nevertheless, slight differences exist between in vivo and in vitro defects (Table 3), namely in the relative amount of the different possible types and also in the local molecular configurations of some of them.

Disclinations are of different type: λ^- in vitro and τ^- in vivo. The most energetic situation (τ^-) is that encountered in chromosomes, whereas it is completely prohibited in vitro.

In vivo, edge dislocations correspond almost exclusively to the addition of only one layer in the structure ($\mathbf{b} = P/2$), whereas in vitro the addition of two layers is also frequent (regardless of the considered DNA length, either 50 nm or polydisperse 50–2000-nm fragments). The core configuration $\tau^-\lambda^+$ is favored in chromosomes as in liquid crystalline phases made of long DNA molecules.

The influence of molecular length is already enlightened by our experiments, since preferred core configurations vary according to the considered length. In vivo, the length of the DNA molecule, that can be considered as "infinite," introduces additional topological constraints, that will not appear in our liquid crystalline sample. Indeed, the liquid crystalline organization of a chromosome-length DNA molecule would require years. Of course, other chromatin components (namely RNA and proteins), should also be taken into consideration to explain such differences. They may for example alter DNA bending as well as its degree of supercoiling, thus facilitating peculiar three-dimensional configurations. The effect of protein addition remains now to be tested in order to progress in the understanding of the chromatin organization.

2) The defects are quite rare in cholesteric germs in vitro, since they tend to move to the surface of the germ and to be eliminated for energetic reasons. In chromosomes of dinoflagellates, which are also cholesteric germs in equilibrium with an isotropic phase, these defects are frequent. They perhaps simply remain trapped in the structure because of the restricted fluidity, but some nuclei possess a high defect content, whereas other do not and, though there is no experi-

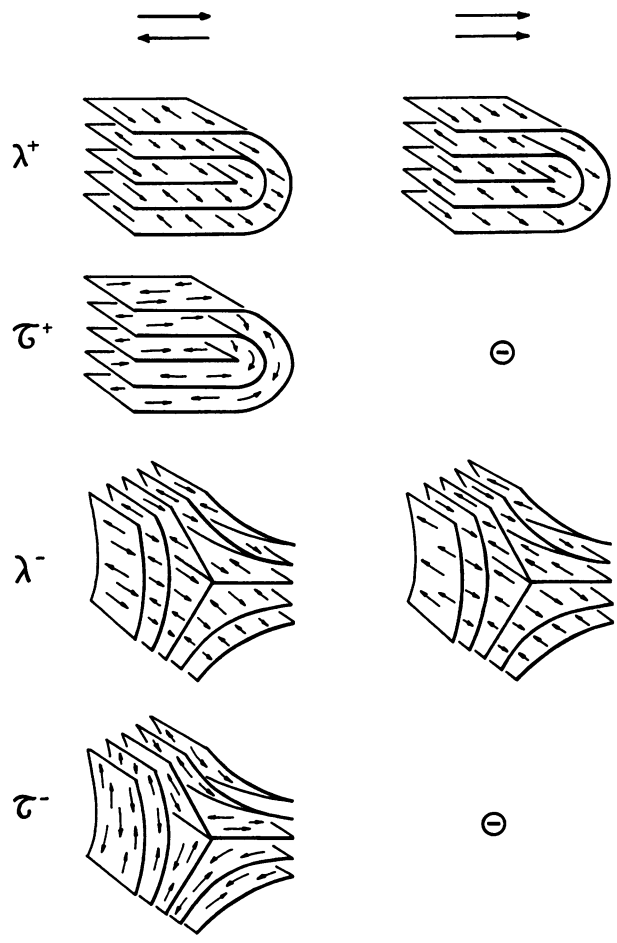

FIGURE 16 Different types of disclinations and their possible occurrence in the two hypotheses presented in Fig. 15. τ^+ and τ^- situations can be observed only if molecules can align antiparallel. λ^- and λ^+ are allowed whatever the constraints of alignments of the DNA molecule.

TABLE 4 Helical pitch in cholesteric chromatin

	P
	nm
Dinoflagellates	
Prorocentrum micans (Livolant, 1980)	180–400
Prorocentrum micans (Soyer and Haapala, 1974)	72–500
Gymnodinium sp. (Zingmark, 1970)	320
Prorocentrum minimum (Fritz and Triemer, 1983)	290
Peridinium cinctum (Spector et al., 1981)	280
Polykrikos (Bradbury et al., 1983)	220
Amphidinium carterae (Oliveira and Huynh, 1989)	192
Amphidinium carterae (Oakley and Dodge, 1979)	160
Blastodinium (Soyer, 1969)	178
Noctiluca (Soyer, 1972)	150
Noctiluca (Soyer, 1970)	136 189
Gonyaulax polyedra (Donner and Rensing, 1984)	150
Oodinium (Cachon and Cachon, 1977)	90
Prorocentrum marialabouriae (Loeblich, 1976)	65–68
Bacteria	
Bacillus thurigiensis (Nishimura et al., 1980)	280
Rhizobium (Gourret, 1978)	193
"Troglophytic prokaryotes" (Cox, 1978)	163
Bacillus subtilis (Ryter, 1963)	149
Escherichia coli (Zusman et al., 1973)	125
Escherichia coli (Gründ, 1974)	112–143
Kinetoplasts	
Bodo (Brugerolle and Mignot, 1979)	133
Sperm nuclei	
Whip scorpion (Phillips, 1976)	>2000*
Fish (Gusse and Chevalier, 1978)	746*
Pleurodele (Picheral, 1971)	70
Stallion (Livolant, 1984)	66
Bull (Koehler, 1966; Plattner, 1971)	50–60
Rabbit (Koehler, 1970)	50

Values of the cholesteric pitch (*P*) as measured on micrographs in sections showing a periodicity characteristic of the cholesteric structure. Only sections devoid of arcs (i.e., normal to the layers) have been taken into consideration.

* Indicative values since they were measured in structures with a diameter smaller than half the helical pitch (*P*/2).

mental evidence, this could be related to the stage of the cell cycle. We may therefore hypothesize that they could be involved in specific biological functions since they correspond to particular molecular configurations. Conversely, they could also correspond to a geometrical solution of a local overcrowding, resulting from the replication of the DNA molecule. Unfortunately, there is not enough experimental data available to choose between these two hypotheses.

3) Defects correspond to particular topological situations. Their analysis provides information about the contraints of alignment of DNA molecules, either in a strictly parallel way, or any way (parallel and antiparallel just as well), these constraints being able to favor or prevent particular functions.

The DNA molecule can be oriented by considering the polarity 3′-5′ of one of the strands chosen arbitrarily. This orientation corresponds for example to a choice of direction to travel along a DNA molecule. The real periodicity of the cholesteric phase depends on the ability of DNA molecules to align either in a strictly parallel way (the period equals P and corresponds to a rotation of 360° of the molecular orientations) or any way, the molecule being able to fold back and forth (the period equals $P/2$ and corresponds to a rotation of 180°) (Fig. 15). The regions devoid of defects do not allow us to answer this question, while defects do. Indeed, in any periodic structure, the value of Burger's vector (**b**) cannot be smaller than the period of the structure itself. The presence of numerous $P/2$ edge dislocations in the cholesteric phases indicates that the real period here equals $P/2$. In theory, defects corresponding to the addition of two layers ($\mathbf{b} = P$) would be the elementary defects if DNA molecules do strictly align in parallel (Fig. 15). Nevertheless, if we consider the core configurations, some of them are also prohibited. Indeed, only disclinations λ^+ and λ^- (which are devoid of molecular discontinuities) can account for a strict alignment of DNA molecules (Fig. 16). Consequently, the strict parallel alignment of DNA molecules is compatible only with $\lambda^-\lambda^+$ dislocations.

These geometrical observations allow us to reanalyze the data presented in Table 3 in which the defects requiring an antiparallel alignment of DNA molecules have been hatched. All dinoflagellate chromosomes defects (except two) follow this rule that eliminates the polytenic models of these chromosomes since polyteny imposes a strict parallel alignment of DNA molecules (46). Besides, topological reasons leads us to understand easily that an infinite DNA molecule cannot be packaged into a cholesteric structure without folding of the molecule, thus raising such defects.

However, the rare $\mathbf{b} = P$ defects could be privileged places for functions requiring a strict parallel alignment of DNA molecules and such topological constraints exist for example in recombination: the first step of the process (synapsis) corresponds to the functional alignment of the recombination sites, thus allowing the subsequent breakage and cross reunion (47), and these sites must be aligned in parallel whether they are direct or inverted along the DNA molecule.

Variations of the helical pitch

As indicated in the Results, the helical pitch P varies in vitro from 200 to 400 nm (with 50-nm DNA fragments and also with sonicated molecules from 50 to 190 nm in length) to more than 5000 nm with an average value in the range of 2200 (39) to 2540 nm (present results). There are numerous examples of chromatin showing a cholesteric organization (48), and, in these materials, the helical pitch varies from about 50 to 450 nm, as estimated by measurements of the periodic patterns on thin sections (Table 4). The smallest helical pitches are observed in sperm nuclei (500–700 Å, depending on the species). In bacteria, P varies from about 1000 to 2800 Å and in dinoflagellate chromosomes from 70 to 450 nm. In these two last groups, P varies with the species and also within a given species according to physiological conditions. The occurrence of small pitch helical phases in vitro reveals that particular experimental conditions can be found to mimic the biological organization. Nevertheless, a systematic study of the influence of different parameters including ionic environment, length, and sequence of DNA fragments, as well as the addition of other chromatin components will in the future allow more relevant comparisons with chromatin organization.

We thank Y. Bouligand and J. L. Sikorav and for their critical comments on the manuscript.

This research was supported by a grant from the Association pour la Recherche sur le Cancer and grant 910909 from the Institut National de le Santá et de la Recherche Mádicale.

REFERENCES

1. Kellenberger, E., E. Carlemalm, E. Sechaud, A. Ryter, and G. de Haller. 1986. Considerations on the condensation and degree of compactness in non-eukaryotic DNA-containing plasmas. *In* Bacterial chromatin. C. O. Guarlerzi and C. L. Pon, editors. Springer Verlag, Berlin and Heidelberg. 11–25.
2. Robinson, C. 1961. Liquid crystalline structures in polypeptide solutions. *Tetrahedron.* 13:219–234.
3. Lerman, L. S. 1973. Chromosomal analogues: long-range order in Y condensed DNA. *Cold Spring Harbor Symp. Quant. Biol.* 38:59–73.
4. Iizuka, E. 1977. Some new findings in the liquid crystals of sodium salt of deoxyribonucleic acid. *J. Physique (Paris)* 9:173–180.
5. Senechal, E., Maret, G., and K. Dransfeld. 1980. Long-range order of nucleic acids in aqueous solutions. *Int. J. Biol. Macromol.* 2:256–262.
6. Livolant, F. 1984. Cholesteric organization of DNA in vivo and in vitro. *Eur. J. Cell Biol.* 33:300–311.
7. Livolant, F. 1986. Cholesteric liquid crystalline phases given by three helical biological polymers: DNA, PBLG and xanthan. A comparative analysis of their textures. *J. Physique (Paris).* 47:1605–1616.
8. Livolant, F. 1987. Precholesteric liquid crystalline states of DNA. *J. Physique. (Paris).* 48:1051–1068.
9. Rill, R. L. 1986. Liquid crystalline phases in concentrated aqueous solutions of Na^+ DNA. *Proc. Natl. Acad. Sci. USA.* 83:342–346.
10. Bouligand, Y., and F. Livolant. 1984. The organization of cholesteric spherulites. *J. Physique (Paris).* 45:1899–1923.
11. Brandes, R., and D. R. Kearns. 1986. Magnetic ordering of DNA liquid crystals. *Biochemistry.* 25:5890–5895.
12. Livolant, F., and Y. Bouligand. 1986. Liquid crystalline phases given by helical biological polymers (DNA, PBLG and xanthan). *J. Physique.* 47:1813–1827.

13. Strzelecka, T. E., and R. L. Rill. 1987. Solid-state ^{31}P NMR studies of DNA liquid crystalline phases. The isotropic to cholesteric transition. *J. Am. Chem. Soc.* 109:4513–4518.
14. Strzelecka, T. E., and R. L. Rill. 1990. A 23 Na-NMR study of sodium-DNA interactions in concentrated DNA solutions at low-supporting electrolyte concentration. *Biopolymers.* 30:57–71.
15. Strzelecka, T. E., Davidson, M. W., and R. L. Rill. 1988. Multiple liquid crystal phases of DNA at high concentrations. *Nature.* 331:457–460.
16. Yevdokimov, Yu. M., S. G. Skuridin, and V. I. Salyanov. 1988. The liquid-crystalline phases of double-stranded nucleic acids in vitro and in vivo. *Liq. Cryst.* 3:1443–1459.
17. Livolant, F., A. M. Levelut, J. Doucet, and J. P. Benoit. 1989. The highly concentrated liquid crystalline phase of DNA is columnar hexagonal. *Nature.* 339:724–726.
18. Livolant, F. 1991. Supramolecular organization of double-stranded DNA molecules in the columnar hexagonal liquid crystalline phase. *J. Mol. Biol.* 218:165–181.
19. Rill, R. L., T. E. Strzelecka, M. W. Davidson, and D. H. Van Winkle. 1991. Ordered phases in concentrated DNA solutions. *Physica A.* 176: 87–116.
20. Bouligand, Y., M. O. Soyer, and S. Puiseux-Dao. 1968. La structure fibrillaire et l'orientation des chromosomes chez les Dinoflagellás. *Chromosoma.* 24:251–287.
21. Rill, R. L., F. Livolant, H. C. Aldrich, and M. W. Davidson. 1989. Electron microscopy of liquid crystalline DNA: direct evidence for cholesteric-like organization of DNA in dinoflagellate chromosomes. *Chromosoma.* 98:280–286.
22. Gourret, J. P. 1978. Description et interprétation des nücláoïdes structurás observás dans les bactároïdes de *Rhizobium. Biol. Cell.* 32:299–306.
23. Lepault, J., J. Dubochet, W. Baschong, and E. Kellenberger. 1987. Organization of double-stranded DNA in bacteriophages: a study by cryo-electron microscopy of vitrified samples. *EMBO J.* 6:1507–1512.
24. Luzzati, V., and A. Nicolaieff. 1959. Etude par diffusion des rayons X aux petits angles des gels d'acide dásoxyribonucláique et de nucláoprotáines. *J. Mol. Biol.* 1:127–133.
25. Luzzati, V., and A. Nicolaieff. 1963. The structure of nucleohistones and nucleoprotamines. *J. Mol. Biol.* 7:142–163.
26. Feughelman, M., R. Langridge, W. E. Seeds, A. R. Stokes, H. R. Wilson, M. H. F. Wilkins, R. K. Barclay, and L. D. Hamilton. 1955. Molecular structure of deoxyribose nucleic acid and nucleoprotein. *Nature.* 175: 834–838.
27. Leforestier, A., and F. Livolant. 1991. Cholesteric liquid crystalline DNA: a comparative analysis of cryofixation methods. *Biol. Cell.* 71: 115–122.
28. Fuller, R. S., J. M. Kaguni, and A. Kornberg. 1981. Enzymatic replication of the origin of the *Escherichia coli* chromosome. *Proc. Natl. Acad. Sci. USA.* 78:7370–7374.
29. Sikorav, J. L., and G. M. Church. 1991. Complementary recognition in condensed DNA: accelerated DNA renaturation. *J. Mol. Biol.* 222: 1085–1108.
30. Escaig, J. 1982. New instruments which facilitate rapid freezing of 83K and 6K. *J. Microsc.* 126:221–229.
31. Livolant, F., and M. F. Maestre. 1988. Circular dichroïsm microscopy of compact forms of DNA and chromatin in vivo and in vitro: cholesteric liquid crystalline phases of DNA and single dinoflagellate nuclei. *Biochemistry.* 27:3056–3068.
32. Iizuka, E., and Y. Kondo. 1979. Magnetic-field orientation of the liquid crystals of polyribonucleotide complexes. *Mol. Cryst. Liq. Cryst.* 51: 285–294.
33. Bouligand, Y. 1972. Recherche sur les textures des états mésomorphes. 2. Les champs polygonaux dans les cholestériques. *J. Physique (Paris).* 33:715–736.
34. Leforestier, A., and F. Livolant. 1992. Distortion of DNA cholesteric liquid crystal quenched at low temperature: geometrical analysis and modelization. *J. Physique II (Paris).* 2:1853–1880.
35. Kláman, M. 1977. Points, Lignes et Parois. Les éditions de Physique, Publs. Orsay (France).
36. Bouligand, Y., P. E. Cladis, L. Liebert, and L. Strzelecki. 1974. Study of sections of polymerized liquid crystals. *Mol. Cryst. Liq. Cryst.* 25: 233–252.
37. Bouligand, Y. 1973. Recherches sur les textures des états mésomorphes. 3. Les plages à éventails dans les cholestériques. *J. Physique.* 34:603–614.
38. Livolant, F., and Y. Bouligand. 1989. Freeze-fractures in cholesteric mesophases of polymers. *Mol. Cryst. Liq. Cryst.* 166:91–100.
39. Van Winkle, D. H., M. W. Davidson, W. X. Chen, and R. L. Rill. 1990. Cholesteric helical pitch of near persistence length DNA. *Macromolecules.* 23:4140–4148.
40. Livolant, F., and A. Leforestier. 1992. DNA mesophases: a structural analysis in polarizing and electron microscopy. *Mol. Cryst. and Liq. Cryst.* 215:47–56.
41. Tsurimoto, T., and K. Matsubara. 1982. Replication of λ dv plasmid in vitro promoted by purified λ O and P proteins. *Proc. Natl. Acad. Sci. USA.* 79:7639–7643.
42. Zimmerman, S. B., and B. Harrison. 1987. Macromolecular crowding increases binding of DNA polymerase to DNA: an adaptative effect. *Proc. Natl. Acad. Sci. USA.* 84:1871–1875.
43. Krasnov, M. A., and N. R. Cozzarelli. 1982. Catenation of DNA rings by topoisomerases. *J. Biol. Chem.* 257:2687–2693.
44. Pheiffer, B. H., and S. B. Zimmerman. 1983. *Nucleic Acids Res.* 11: 7853–7871.
45. Grasso, D., S. Fasone, and C. L. Rosa. 1991. A calorimetric study of the different thermal behaviour of DNA in the isotropic and liquid-crystalline states. *Liquid Crystals.* 9:299–305.
46. Livolant, F., and Y. Bouligand. 1978. New observations on the twisted arrangement of dinoflagellate chromosomes. *Chromosoma.* 78:21–44.
47. Benjamin, H. W., and N. R. Cozzarelli. 1986. DNA-directed synapsis in recombination: slithering and randon collision of sites. *Proc. Robert A. Welch. Found. Conf. Chem. Res.* 29:107–126.
48. Livolant, F. 1991. Ordered phases of DNA in vivo and in vitro. *Physica A.* 176:117–137.
49. Baeza, I., P. Gariglio, L. Rangel, P. Chavez, L. Cervantes, C. Arguello, C. Wong, and C. Montañez. Electron microscopy and biochemical properties of polyamines compacted DNA. *Biochemistry.* 26:1387–1392.